DOI: 10.1002/ejic.201000524

Terahertz Time Domain Spectroscopy to Detect Low-Frequency Vibrations of Double-Walled Carbon Nanotubes

Sunil Kumar,[a] Natrajan Kamaraju,[a] Alexander Moravsky,[b] R. O. Loutfy,[b] Marc Tondusson,[c] Eric Freysz,[c] and Ajay Kumar Sood*[a]

Keywords: Carbon / Nanotubes / Time-resolved spectroscopy / Dielectric function / Low-frequency phonons

We have measured the frequency-dependent real index of refraction and extinction coefficient (and hence the complex dielectric function) of a free-standing double-walled carbon nanotube film of thickness 200 nm by using terahertz time domain spectroscopy in the frequency range 0.1 to 2.5 THz. The real index of refraction and extinction coefficient have very high values of approximately 52 and 35, respectively, at 0.1 THz, which decrease at higher frequencies. Two low-frequency phonon modes of the carbon nanotubes at 0.45 and 0.75 THz were clearly observed for the first time in the real and imaginary parts of the complex dielectric function along with a broad resonance centred at around 1.45 THz, the latter being similar to that in single-walled carbon nanotubes assigned to electronic excitations. Our experiments bring out a possible application of double-walled carbon nanotube films as a neutral density filter in the THz range.

Introduction

Carbon nanotubes are of great interest, both theoretically and experimentally, in optoelectronic applications, particularly in the gigahertz (GHz) to terahertz (THz) frequency range. They are good candidates for fabricating devices such as THz emitters,[1] detectors,[2] filters,[3] polarizers[4] and microwave detectors.[5] In recent years, THz time domain spectroscopy (THz-TDS), which uses subpicosecond THz pulses, has become a very effective technique to make contactless measurements of the optical and electrical properties of materials. THz properties of carbon nanotubes (CNTs) have been studied by using THz-TDS.[6–11] For single-walled carbon nanotubes (SWNTs) dispersed in a carboxymethylcellulose matrix, the real and imaginary parts of the complex dielectric function increase at frequencies below 5 THz, reaching a high value of approximately 80 at 0.2 THz and showing a broad maximum at approximately 3 THz in the real part of the conductivity, attributed to the curvature-induced electronic band gap in quasi-metallic carbon nanotubes.[6] Similar results have been obtained for films of SWNTs mixed with methylcellulose binder[7] and a SWNT film on a quartz substrate.[8] However, the broad feature in the real part of the conductivity observed between 1 and 3 THz has been assigned to phonon resonances.[7,8] A recent study[9] attributes the broad feature at approximately 4.5 THz in a SWNT film to an electronic resonance. A comparison of SWNTs and double-walled carbon nanotubes (DWNTs) mixed with KBr powder shows that the real (n) and imaginary (K) parts of the complex refractive index, $n^* = n + iK$, are smaller for DWNTs.[10] In contrast, for a free-standing multiwalled carbon nanotube (MWNT) film of 89 μm thickness, n and K were shown to be frequency-independent in the range 0.05 to 0.4 THz.[11]

In this paper, we report on the THz dielectric response of a 200 nm thick free-standing DWNT film in the 0.1–2.5 THz frequency range measured by THz-TDS in the transmission mode. We observe for the first time two resonances at 0.45 and 0.75 THz, attributed to the low-frequency vibrational modes of the nanotubes, already predicted theoretically for SWNTs[12–16] and DWNTs[17] but not observed directly so far in either absorption or scattering experiments. However, these low-frequency phonons have been invoked in interpreting the very low temperature specific heat data[18] and enhanced phonon density of states[19] in CNTs as compared to graphite. These two-phonon bands are superimposed on a broad background centred at approximately 1.45 THz. We emphasize that the 200 nm thick DWNT film in our studies allows only less than 50% of the transmittance in both the time and the frequency domain and hence can be a useful material for applications in thickness-dependent real-time control, spectral modulation and radiation shielding of THz electromagnetic waves.

Results and Discussion

Figure 1 (a) shows the temporal electric field, $E(t)$, associated with the THz wave transmitted through the DWNT

[a] Department of Physics and Centre for Ultrafast Laser Applications, Indian Institute of Science, Bangalore 560012, India
E-mail: asood@physics.iisc.ernet.in
[b] Materials and Electrochemical Research Corporation, Tucson, AZ, USA
[c] Université de Bordeaux I, CPMOH, UMR CNRS 5798, 351, Cours de la liberation, 33405 Talence cedex, France

film (thick line) along with the electric field recorded without the sample (thin line). The measured temporal signal contains the amplitude and the phase information of the electric field associated with the THz pulse. Fast Fourier transform (FFT) gives direct access to the amplitude and phase at different spectral components of the THz electromagnetic wave. Therefore, from THz-TDS, the real and imaginary parts of the complex refractive index are obtained without invoking the Kramers–Kronig analysis.

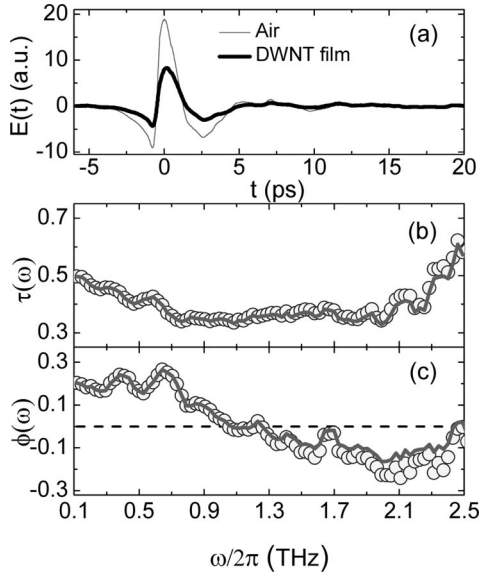

Figure 1. (a) THz time domain signal recorded in air and with the DWNT film; (b) amplitude $\tau(\omega)$ and (c) phase $\phi(\omega)$ of the spectral transmission coefficient of the film. Circles in (b) and (c) are the experimentally measured values and the continuous lines are the results of ellipsometric modelling (see text).

It can be observed in Figure 1(a) that the film cuts almost 50% of the amplitude of the THz temporal pulse without affecting the temporal width. In the frequency domain, the amplitude, $\tau(\omega)$ [Figure 1(b)], of the spectral transmission coefficient, $T(\omega)$, varies between 35 and 50% in the frequency range 0.1 to 2.0 THz. This indicates possible application of the free-standing DWNT film as neutral density filter in the THz spectral range. The attenuation coefficient of such DWNT films can be easily adjusted by changing their thickness and, hence they may be used for real-time control and manipulation of THz radiation. The spectral phase, $\phi(\omega)$ [Figure 1(c)], changes sign from positive to negative at approximately 1.3 THz, which is indicative of a resonance response around this frequency.

In calculating the complex index of refraction of an optically thin film by THz-TDS, one has to take into account the Fabry–Perot echoes from the finite thickness of the film superimposed with the main THz pulse, thus giving the transmission coefficient of the film in Equation (1).[21]

$$T(\omega) = \tau(\omega)\exp[i\phi(\omega)] = \frac{t_{12}(\omega)t_{23}(\omega)\exp[i\beta(\omega) - i\omega d/c]}{1 + r_{12}(\omega)r_{23}(\omega)\exp[2i\beta(\omega)]} \quad (1)$$

Here $\beta(\omega) = 2n^*(\omega)\pi d/\lambda$ is the phase shift sensed by each THz wavelength, λ, propagating through the thin film of thickness d, ω is angular frequency and c is the speed of light in vacuum; (r_{12}, t_{12}) and (r_{23}, t_{23}) are the Fresnel coefficients for the reflection and transmission from the front and the back surfaces of the thin film. The thickness of the film is sufficiently small relative to the wavelength of the THz radiation in the experiment ($d/\lambda \approx 10^{-3}$), and hence the term $\exp(-i\omega d/c)$ in the numerator of Equation (1) can be ignored for simplicity. At normal incidence, the Fresnel coefficients have simple expressions: $r_{kl} = (n_k - n_l)/(n_k + n_l)$ and $t_{kl} = 2n_k/(n_k + n_l)$, where k, l = 1, 2, 3, and $k \neq l$. In our experiments, the sample was suspended in air between the THz emitter and detector and hence $n_1 = n_3 = 1$. Since $\tau(\omega)$ and $\phi(\omega)$ are known experimentally [Figure 1(b) and 1(c)], $n^*(\omega)$ can be deduced by solving Equation (1) numerically.[21] Here we adopt the methodology well known for ellipsometry, taking into account the known thickness of the film. To briefly summarize the procedure, a new variable, $\eta(\omega) = \exp[i\beta(\omega)]$, is introduced, allowing to rewrite Equation (1) as $A\eta^2 + B\eta + C = 0$, which can be solved for $\eta(\omega)$. Here $A(\omega) = [n^*(\omega) - 1]T(\omega)$, $B(\omega) = 4n^*(\omega)$ and $C(\omega) = -[n^*(\omega) - 1]^2T(\omega)$. As d is a real number, a correct solution for $n^*(\omega)$ must satisfy $\mathrm{Re}[\ln\eta(\omega)/n^*(\omega)] = 0$ and $\mathrm{Im}[\ln\eta(\omega)/n^*(\omega)] - \omega d/c = 0$. In the ($n$, K) parameter space, these two equations represent two planar contours, whose crossing point is the correct solution for n and K at a particular ω. The results are shown in Figure 2(a). To check the validity of our procedure, we substitute values of $n(\omega)$ and $K(\omega)$ obtained in Equation (1) and calculate $\tau(\omega)$ and $\phi(\omega)$ as shown by the solid lines in Figures 1(b) and (c). It can be seen that the calculated values match very well the experimental data (circles), thus validating our procedure.

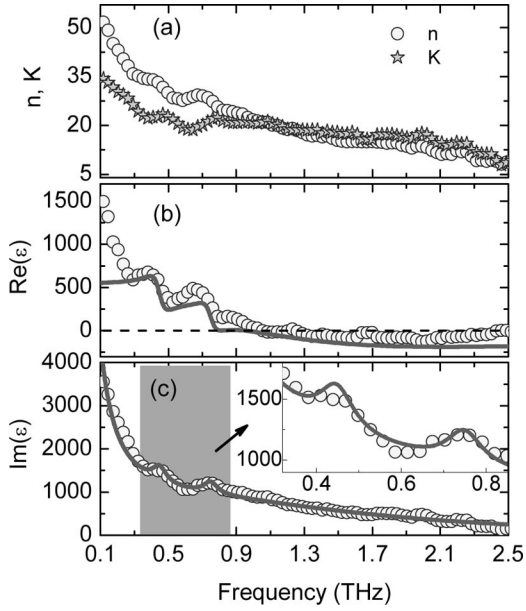

Figure 2. (a) Real index of refraction $n(\omega)$ and extinction coefficient $K(\omega)$, (b) Re(ε) and (c) Im(ε). Continuous lines are the fits of the experimental data to Equation (2), with fitting parameters presented in Table 1.

Figure 2(a) shows that the real index of refraction, n, decreases monotonically from 52 at 0.1 THz to 5 at 2.5 THz, while the extinction coefficient, K, varies from 35 to 5 in the same spectral window. Furthermore, n and K cross over at a frequency $\nu = \omega/2\pi$, which is approximately 1.3 THz, signalling a resonance around that frequency. The real and imaginary parts of the dielectric function, $\mathrm{Re}(\varepsilon) = n^2 - K^2$ and $\mathrm{Im}(\varepsilon) = 2nK$, are shown by circles in Figures 2(b) and (c), respectively. We note that both $\mathrm{Re}(\varepsilon)$ and $\mathrm{Im}(\varepsilon)$ increase to very high values at low frequencies, much higher than those reported for SWNT films.[6–10] We fit the measured dielectric function with a combined Drude–Lorentz oscillator model given in Equation (2).

$$\varepsilon(\omega) = \varepsilon_\infty - \frac{{\omega_p}^2}{\omega(\omega + i\Gamma)} + \sum_{k=1}^{3} \frac{{F_k}^2}{{\omega_k}^2 - \omega^2 - i\omega\gamma_k} \quad (2)$$

Here, ω_p and Γ are the plasma frequency and the damping constant of the Drude oscillator, respectively. The parameter F_k is the oscillator strength of the resonance at frequency ω_k with lifetime broadening γ_k; ε_∞ is the high-frequency dielectric constant of the DWNT film. The summation over three values of k as dictated by the fit to the data represents three modes, two being phonons and one electronic resonance. The solid line in Figure 2(c) is the result fitted with parameters given in Table 1 along with $\varepsilon_\infty = 2.5$. With these parameters, $\mathrm{Re}(\varepsilon)$ is calculated as given by the solid line in Figure 2(b). We note that the fit for $\mathrm{Re}(\varepsilon)$ is not as good as that for $\mathrm{Im}(\varepsilon)$. The parameters for the Drude part are $\omega_p/2\pi = 17$ THz (energy = 70 meV) and $\Gamma/2\pi = 0.65$ THz. The latter implies a carrier collision time, τ (= $1/\Gamma$), of approximately 250 fs and a scattering length, l (ca. $v_F\tau$, where $v_F = 10^6\ \mathrm{ms}^{-1}$ is the Fermi velocity), of approximately 250 nm, a fraction of the nanotube length. The zero-frequency conductivity, $\sigma(0) = \varepsilon_0{\omega_p}^2/\Gamma$, where ε_0 is the vacuum permittivity, is approximately $2.5 \times 10^4\ \Omega^{-1}\mathrm{m}^{-1}$, which corresponds to an average carrier density, η [= $\sigma(0)m/e^2\tau$], of approximately $3.5 \times 10^{24}\ \mathrm{m}^{-3}$.

The negative values of $\mathrm{Re}(\varepsilon)$ at frequencies beyond 1.3 THz [Figure 2(b)] are due to an overdamped resonance at frequency $\omega_{k=3}/2\pi = 1.45$ THz and Lorentz oscillator strength ($F_k/2\pi$) of approximately 48 THz, which dominates the free carrier response at smaller frequencies [manifested by the large positive values of $\mathrm{Re}(\varepsilon)$]. This feature can be attributed to localized absorption in the direct transition across the electronic band gap in quasi-metallic tubes,[22,23] similar to the resonance observed for SWNTs between 3 and 5 THz.[6,9] A large spectral width, $\gamma_{k=3}/2\pi = 3$ THz, reflects the broad distribution of gap energies.

Additionally, the dispersions in $\mathrm{Re}(\varepsilon)$ and the corresponding peaks in $\mathrm{Im}(\varepsilon)$ at the frequencies 0.45 THz and 0.75 THz have similar oscillator strengths and line widths (see Table 1). These can be attributed to the low-frequency phonons of CNTs. For example, the out-of-phase combinations of four acoustic modes (frequency $\omega \to 0$ as wave vector $\mathbf{q} \to 0$ at the centre of the Brillouin zone) of the two individual single-walled tubes have been predicted to be infrared-active optical modes[17] and can have frequencies of approximately 1 THz associated with the longitudinal and twisting rigid layer modes of a DWNT with an outer tube diameter of approximately 2 nm. It may be noted that these spectral features are observed by us for the first time for CNTs.

Table 1. Parameters of Equation (2) obtained from the fitting of the experimental complex dielectric function.

$\omega_k/2\pi$ (THz)	$\gamma_k/2\pi$ (THz)	$F_k/2\pi$ (THz)
0.45 ± 0.01	0.11 ± 0.03	2.0 ± 0.2
0.75 ± 0.02	0.11 ± 0.04	2.1 ± 0.2
1.45 ± 0.02	3.03 ± 0.08	48.5 ± 1.0

Conclusions

THz-TDS has been used to observe directly two low-frequency phonons at 0.45 and 0.75 THz superimposed on a broad electronic resonance centred at approximately 1.45 THz for a free-standing DWNT film. The temporal and spectral characteristics of the DWNT film (Figure 1) suggest their possible applications in real-time control and manipulation of THz radiation and as THz neutral density filters.

Experimental Section

Free-standing DWNT films of approximate thickness 200 nm, as measured with atomic force microscopy (AFM), were grown by high-temperature chemical vapour deposition and characterized by transmission electron microscopy.[20] The atomic force micrograph of the film is shown in Figure 3(a). The Raman spectrum of the

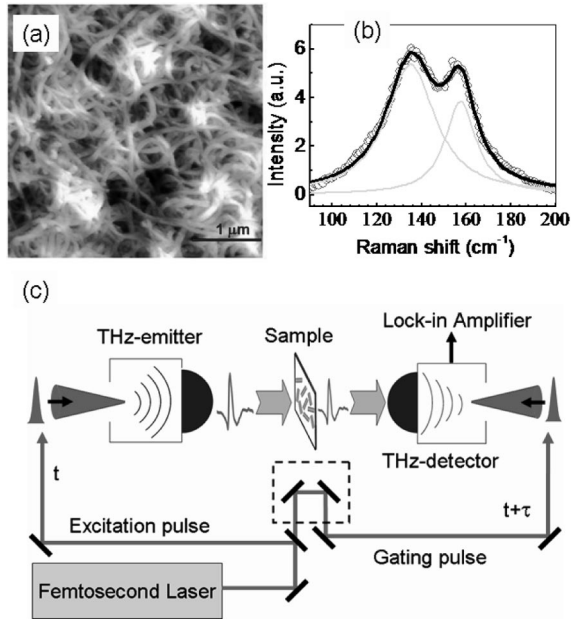

Figure 3. (a) Atomic force micrograph and (b) Raman spectrum of a thin free-standing DWNT film of approximate thickness 200 nm. (c) Schematic of the THz-TDS set-up in transmission mode using photoconductive antennas as THz emitter and a detector excited by 100 fs laser pulses centred at 800 nm.

film [Figure 3(b)] shows two radial breathing modes (RBMs) at 135 and 157 cm^{-1}, corresponding to outer tube diameters of 1.95 and 1.65 nm, respectively. We have used the photoconductive switching technique for THz-TDS shown schematically in Figure 3(c). The THz emitter and detector consist of microstrip antennas integrated with low-temperature grown GaAs photoconductors and Si lenses. The emitter and the detector were driven by 100 fs laser pulses from a 76 MHz continuously mode-locked Ti/sapphire oscillator at an average power of 50 and 38 mW, respectively. The beams were focused onto the antennas by using 12.5 cm focal length lenses. The THz generation was modulated and detected at a lock-in frequency of 34.9 kHz. The free-standing thin film, supported on a 8 mm diameter copper O-ring, was placed normal to the incident THz beam between the two antennas (kept 15 cm apart) but closer to the detector. Our set-up has a good signal-to-noise (S/N) ratio of about 1000:1 at 0.8 THz.

Acknowledgments

A. K. S. thanks the Department of Science and Technology (DST) and E. F. thanks Centre National de la Recherche Scientifique (CNRS) for financial assistance. S. K. acknowledges the University Grant Commission (UGC) for a Senior Research Fellowship. This work was partially supported by the Indo-French Network P2R program. We thank Dr. Anindya Das for the Raman spectrum and AFM image of the DWNT film.

[1] O. V. Kibis, M. R. Da Costa, M. E. Portnoi, *Nano Lett.* **2007**, *7*, 3414–3417.
[2] K. Fu, R. Zannoni, C. Chan, S. H. Adams, J. Nicholson, E. Polizzi, K. S. Yngvessona, *Appl. Phys. Lett.* **2008**, *92*, 033105–033107.
[3] M. A. Seo, J. H. Yim, Y. H. Ahn, F. Rotermund, D. S. Kim, S. Lee, H. Lim, *Appl. Phys. Lett.* **2008**, *93*, 231905–231907.
[4] L. Ren, C. L. Pint, L. G. Booshehri, W. D. Rice, X. Wang, D. J. Hilton, K. Takeya, I. Kawayama, M. Tonouchi, R. H. Hauge, J. Kono, *Nano Lett.* **2009**, *9*, 2610–2613.
[5] F. R. Morales, R. Zannoni, J. Nicholson, M. Fishetti, K. S. Yngvesson, J. Appenzeller, *Appl. Phys. Lett.* **2006**, *89*, 083502–083504.
[6] H. Nishimura, N. Minami, R. Shimano, *Appl. Phys. Lett.* **2007**, *91*, 011108–011110.
[7] T. I. Jeon, K. J. Kim, C. Kang, I. H. Maeng, J. H. Son, K. H. An, J. Y. Lee, Y. H. Lee, *J. Appl. Phys.* **2004**, *95*, 5736–5740.
[8] C. Kang, I. H. Maeng, S. J. Oh, S. C. Lim, K. H. An, Y. H. Lee, J. H. Son, *Phys. Rev. B* **2007**, *75*, 085410–085414.
[9] T. Kampfrath, L. Perfetti, K. von Volkmann, C. M. Aguirre, P. Desjardins, R. Martel, C. Frischkorn, M. Wolf, *Phys. Status Solidi B* **2007**, *244*, 3950–3954.
[10] I. Maeng, C. Kang, S. J. Oh, J. H. Son, K. H. An, Y. H. Lee, *Appl. Phys. Lett.* **2007**, *90*, 051914–051916.
[11] Z. Wu, L. Wang, Y. Peng, A. Young, S. Seraphin, H. Xin, *J. Appl. Phys.* **2008**, *103*, 094324–094326.
[12] M. J. Leamy, A. DiCarlo, *Comput. Meth. Appl. Mech. Eng.* **2009**, *198*, 1572–1584.
[13] H. Suzuura, T. Ando, *Phys. Rev. B* **2002**, *65*, 235412–235426.
[14] G. D. Mahan, *Phys. Rev. B* **2002**, *65*, 235402–235408.
[15] G. D. Mahan, G. S. Jeon, *Phys. Rev. B* **2004**, *70*, 075405–075415.
[16] L. Chico, R. P. Alvarez, C. Cabrillo, *Phys. Rev. B* **2006**, *73*, 075425–075431.
[17] M. Damnjanovic, E. Dobardzic, I. Milosevic, T. Vukovic, B. Nikolic, *New J. Phys.* **2003**, *5*, 148.1–148.15.
[18] J. Hone, B. Batlogg, Z. Benes, A. T. Johnson, J. E. Fischer, *Science* **2000**, *289*, 1730–1733.
[19] S. Rols, Z. Benes, E. Anglaret, J. L. Sauvajol, P. Papanek, J. E. Fischer, G. Coddens, H. Schober, A. J. Dianoux, *Phys. Rev. Lett.* **2000**, *85*, 5222–5225.
[20] V. Gadagkar, S. Saha, D. V. S. Muthu, P. K. Maiti, Y. Lansac, A. Jagota, A. Moravsky, R. O. Loutfy, A. K. Sood, *J. Nanosc. Nanotech.* **2007**, *7*, 1753–1759.
[21] L. Duvillaret, F. Garet, J. L. Coutaz, *IEEE J. Sel. Top. Quantum Electron.* **1996**, *2*, 739–746.
[22] M. Ouyang, J. L. Huang, C. L. Cheung, C. M. Lieber, *Science* **2001**, *292*, 702–705.
[23] A. Ugawa, A. G. Rinzler, D. B. Tanner, *Phys. Rev. B* **1999**, *60*, (R)11305–11308.

Received: May 12, 2010
Published Online: August 16, 2010

